


RESEARCH ARTICLE

Using large ensemble modelling to derive future changes in mountain specific climate indicators in a 2 and 3°C warmer world in High Mountain Asia

P. N. J. Bonekamp¹  | N. Wanders¹ | K. van der Wiel² | A. F. Lutz¹ | W. W. Immerzeel¹

¹Department of Physical Geography, Utrecht University, Utrecht, The Netherlands

²Research and Development - Weather and Climate Modelling, Royal Netherlands Meteorological Institute, de Bilt, The Netherlands

Correspondence

P. N. J. Bonekamp, Department of Physical Geography, Utrecht University, Utrecht, The Netherlands.
Email: p.n.j.bonekamp@uu.nl

Funding information

ERC Horizon 2020 Framework Programme, Grant/Award Number: 676819; Nederlandse Organisatie voor Wetenschappelijk Onderzoek, Grant/Award Numbers: 016.181.308, 016.Veni.181.049, ALWCL.2016.2

Abstract

Natural disasters in High Mountain Asia (HMA) are largely induced by precipitation and temperatures extremes. Precipitation extremes will change due to global warming, but these low frequency events are difficult to analyse using (short) observed time series. In this study, we analysed large 2000 year ensembles of present day climate and of a 2 and 3°C warmer world produced with the EC-Earth model. We performed a regional assessment of climate indicators related to temperature and precipitation (positive degree days, accumulated precipitation, [pre- and post-] monsoon precipitation), their sensitivity to temperature change and the change in return periods of extreme temperature and precipitation in a 2 and 3°C warmer climate. In general, the 2°C warmer world shows a homogeneous response of changes in climate indicators and return periods, while distinct differences between regions are present in a 3°C warmer world and changes no longer follow a general trend. This non-linear effect can indicate the presence of a tipping point in the climate system. The most affected regions are located in monsoon-dominated regions, where precipitation amounts, positive degree days, extreme temperature, extreme precipitation and compound events are projected to increase the most. Largest changes in climate indicators are found in East Himalaya, followed by the Hindu Kush and West and Central Himalaya regions. Western regions will experience drier summers and wetter winters, while monsoon dominated regions drier winters and wetter summers and northern regions a wetter climate year round. We also found that precipitation increases in HMA in a 3°C warmer world are substantially larger (13%) compared to the global average (5.9%). Additionally, the increase in weather extremes will exacerbate natural hazards with large possible impacts for mountain communities. The results of this study could provide important guidance for formulating climate change adaptation strategies in HMA.

This is an open access article under the terms of the Creative Commons Attribution-NonCommercial-NoDerivs License, which permits use and distribution in any medium, provided the original work is properly cited, the use is non-commercial and no modifications or adaptations are made.

© 2020 The Authors *International Journal of Climatology* published by John Wiley & Sons Ltd on behalf of Royal Meteorological Society.

KEYWORDS

climate change, compound events, EC-Earth, High Mountain Asia, large ensemble modelling, mountain, return periods, weather extremes

1 | INTRODUCTION

High Mountain Asia (HMA) is home to the largest reservoir of fresh water outside the poles and 10 major river basins originate in this region. The largest water towers of the world can be found here, of which many are extremely vulnerable to climate change (Immerzeel *et al.*, 2020). In total 1.9 billion people are dependent on the rivers' water resources for irrigation, domestic use and hydropower (Wester *et al.*, 2019), and water demand will further increase in the future (Wijngaard *et al.*, 2018; Biemans *et al.*, 2019).

A global average temperature rise of 1.5°C compared to preindustrial levels implies 2.1°C warming in HMA (Kraaijenbrink *et al.*, 2017) and extreme scenarios would even result in a regional temperature rise up to 5.8°C (RCP8.5; Lutz *et al.*, 2018). Even if the ambitious target of 1.5°C is met, one third of the glacier ice volume would melt by the end of the century (Kraaijenbrink *et al.*, 2017). Because of the buffering role of the cryosphere, glacier and snow melt currently contribute 60% of the water used for irrigation in the Indus during the pre-monsoon season (Biemans *et al.*, 2019). A decrease in melt water availability could therefore have significant implications for agricultural production, hydropower production and human health. Asia has the largest occurrence of natural disasters globally largely caused by hydro-meteorological events. In Asia in the period 2000–2008 52.3% of economic damages is caused by meteorological disasters (Vos *et al.*, 2010).

Understanding the effect of climate change on the magnitude and return periods of extreme precipitation and temperature events is important for assessing impacts on hydropower production and occurrence of natural hazards such as floods, land slides, glacier lake outburst floods and debris flows in HMA (Lutz *et al.*, 2013; Tariq *et al.*, 2014). Natural risk is the interplay between weather hazards, vulnerability and exposure of people, infrastructure and the environment. Extreme weather causes a weather hazard (e.g., landslide or flood) when something or someone is exposed to this hazard and is vulnerable (Aznar-Siguan and Bresch, 2019). Extreme events are normally studied by analysing long time-series or by modelling the tail of the distribution with a statistical approach or extrapolation. Both approaches have limitations as current observational records are short (van der Wiel *et al.*, 2019). Consequently, the statistical significance of results decreases with increasing return periods and often relies on an assumption of stationarity. Furthermore,

when extrapolating the tail of the observational record, assumptions are made regarding the distribution of extremes, which is uncertain for events with a high return period and might change in a future climate.

In order to attribute specific events to climate change, natural climate variability should be disentangled from human-induced climate change. This is challenging as both processes together dynamically drive specific weather events (Trenberth *et al.*, 2015; Hauser *et al.*, 2017). Another method to investigate future weather is to analyse how specific current day (extreme) events will change in the future (Hazeleger *et al.*, 2015). This approach provides important insights in how climate may amplify specific extreme events, however such an approach cannot be used as a probabilistic projection.

An approach to overcome problems with non-stationarity and limited sample size in CMIP model simulations is to use a general circulation model (GCM) to generate long time-series of weather variables given a fixed anthropogenic forcing, by perturbing the boundary conditions. This method called large-ensemble climate simulations can provide long time-series of extreme events in a changing climate and thus provide a unique opportunity to statistically quantify extreme events with a low recurrence interval. In this study we use the large ensemble modelling method in HMA to analyse extreme events using a 2000 year simulation for present and for a 2 and 3°C warmer world respectively (van der Wiel *et al.*, 2019).

In this study we focus on analysing differences between the present-day climate and the 2 and 3°C warmer world for several climate indicators that control the cryosphere (glacier and snow melt and snow fall). In addition, we analyse differences in extreme precipitation and temperature, which are the key drivers for natural hazards such as landslides, avalanches and floods. This work can provide important guidance for formulating climate change adaptation policies.

2 | METHODS

In order to quantify meteorological extremes, data from three large ensembles were analysed: for present day (PD) climate and for a two degrees (2C) and three degrees (3C) warmer world. The large ensembles are performed with the fully coupled EC-Earth global climate model

v2.3 (Hazeleger *et al.*, 2012). The EC-Earth model configuration is the same as in Coupled Model Intercomparison Project phase 5 (CMIP5; Taylor *et al.*, 2012). The ensembles represent three climatic periods with different global mean surface temperature. The PD ensemble has a global mean surface temperature equal to the observed temperatures in the period 2011–2015 (James *et al.*, 2017; van der Wiel *et al.*, 2019). The 2C and 3C ensembles have a global mean surface temperature with 2 and 3°C increase relative to the pre-industrial period (1851–1899).

To generate the large ensembles, a combination of differing initial conditions and atmospheric perturbations was used. Initial conditions were provided by 16 long transient RCP8.5 simulations (1860–2100). From each of these simulations 25 members were branched off, in which atmospheric perturbations were introduced by means of stochastic parameterisations (Buizza *et al.*, 1999). Each member was integrated for 5 years, we assume no climate change effects occur in this 5-year period. The large ensembles thus consist of $16 \times 25 \times 5 = 2000$ years of simulated data. As noted, the 5-year simulation period for each large ensemble was chosen based on a target mean value of global mean surface temperature in the original transient RCP8.5 simulations (extensive details are provided in the supporting information of van der Wiel *et al.*, 2019). The dataset has a global coverage with a spatial resolution of 1.1° and has been used before to assess extreme river discharge under +2 °C global warming (van der Wiel *et al.*, 2019) and extreme heat occurrence in India (Nanditha *et al.*, 2020).

Precipitation was bias-corrected and downscaled to a 0.5° spatial resolution using statistical bias-correction and bicubic spatial downscaling. Precipitation is adjusted for drizzle, which is a common problem in global circulation models (Dai, 2006) and can have significant implications when analysing droughts and dry spells when not corrected. The monthly accumulated precipitation of EC-Earth for each grid cell is matched with monthly sums and the number of wet days in ERA-INTERIM for the PD simulations. These correction factors of wet bias cut off and volume are then linearly interpolated between months to avoid sudden shifts in bias-corrected precipitation. Afterwards, the average daily interpolated correction factors are applied to the two and three degrees warmer large ensembles assuming the model bias in EC-Earth is stationary in time and space under global warming. This bias correction is applied stationary in time, however its real behaviour for the future is unknown and could be more complex.

Temperature was also bias corrected and downscaled with ERA-INTERIM data on a pixel level to produce a 0.5° dataset. A statistical bias-correction allows for elevation corrected downscaling that ensures that monthly

statistics of the PD period match the ERA-INTERIM monthly averages. By taking the high-resolution temperature distribution from ERA-INTERIM we can estimate the sub-pixel distribution for each EC-Earth cell and correct for regional temperature gradients. Following the same procedure as for precipitation, we linearly interpolate the monthly correction factors to a daily temporal resolution. All analyses in this paper are performed with the bias-corrected, downscaled meteorological datasets using the daily temporal resolution of the simulations.

2.1 | Climate indicators

Various climate indicators are analysed to identify sensitive regions in HMA, which either are important for cryospheric processes, monsoon water supply and/or extremes:

1. Positive degree days (PDDs): the annual sum of positive degrees ($T > 0^{\circ}\text{C}$) derived from daily mean temperature. The PDD sum is a measure of the glacier and snow melt potential.
2. Snow: accumulated precipitation for average daily temperature below 0°C . This indicator is important for glacier accumulation, as the total amount of snow controls the glacier accumulation.
3. Pre-monsoon precipitation: precipitation sum between April 1 and June 1. During pre-monsoon irrigation is largely dependent on glacier and snow melt (up to 60% in the Indus basin). Changes in precipitation during this season may compensate for a decrease in melt in the future.
4. Monsoon precipitation: precipitation sum between June 1 and October 1. Glaciers in the Himalaya are characterized by synchronous ablation and accumulation regimes and a change in monsoon precipitation could have implications for the glacier mass balance. Second, shifts in monsoon strength exert a strong control on regional water availability.
5. Post-monsoon precipitation: precipitation sum between October 1 and December 1. The post-monsoon is typically a dry season and precipitation changes in this shoulder season are important for agriculture and hydropower production.
6. 95th percentile of temperature and precipitation: Extreme temperature and precipitation events, defined as the 95th percentile values in the distributions of daily averaged temperature and precipitation values. Extreme precipitation and temperature control landslides, avalanches, floods and heat waves.
7. Compound events: when both precipitation and temperature are higher than their 95th percentile values

in PD climate. Extreme events with both high precipitation amounts and temperature have implications for natural hazards such (melt) water floods and avalanches.

Return periods are calculated using the 2000 year empirical distribution for precipitation and temperature for the PD, 2C and 3C scenarios. For the analysis we use the same regional sub-division as used for the Randolph Glacier Inventory (RGI; RGI Consortium, 2017; Figure 1). PDDs and accumulated solid precipitation are only calculated for glacier grid cells (RGI Consortium, 2017) or for grid cells that are snow covered for at least a month a year (Hall and Riggs, 2015).

3 | RESULTS AND DISCUSSION

3.1 | Performance of EC-Earth in HMA

The complex topography in combination with a complex interplay of monsoon and westerly circulation systems affect the seasonality, amount and spatial distribution of precipitation in HMA. As a result, there is a very large spread between different commonly used gridded datasets (reanalysis, model simulations, satellite or gridded data sets; Palazzi *et al.*, 2013). In the absence of station data it is therefore impossible to identify an optimal precipitation dataset to be used as a reference.

In order to validate the corrected EC-Earth dataset in HMA the average annual cycle of temperature and precipitation of 5 year of TRMM (Huffman *et al.*, 2007), GPM (Huffman *et al.*, 2014), ERA5 data (Copernicus Climate Change Service, 2017; 2011–2015) and the bias corrected EC-Earth are shown in Figure 2. Five years were selected because the PD EC-Earth simulations are aimed to reflect the current climatology and thus comparing to a longer period would lead to inclusion of trends. By making a spatially aggregated evaluation of the HMA region, we reduce the effect of local extremes occurring in ERA5 in those years. For a region-specific comparison reference is made to Figure S1. Temperature in both datasets shows good agreement, and the simulated precipitation shows reasonable agreement. The observed precipitation bias in the bias corrected EC-Earth dataset is -54% and the temperature bias is -0.3°C compared to ERA5. GPM has a yearly precipitation sum bias of -11% and TRMM 0% . These biases are well within the range of uncertainty in temperature and precipitation over HMA. We therefore conclude that the seasonality of temperature and precipitation are captured satisfactory by EC-Earth as was also found in a comparison study between ERA-INTERIM and (non-bias-corrected) EC-Earth in a similar region (Palazzi *et al.*, 2013).

The original EC-Earth is wetter compared to different satellite derived products (Palazzi *et al.*, 2013), while the bias corrected EC-Earth data are well in line with the satellite products GPM and TRMM (Figure 2). Comparison between products is complicated as satellite products

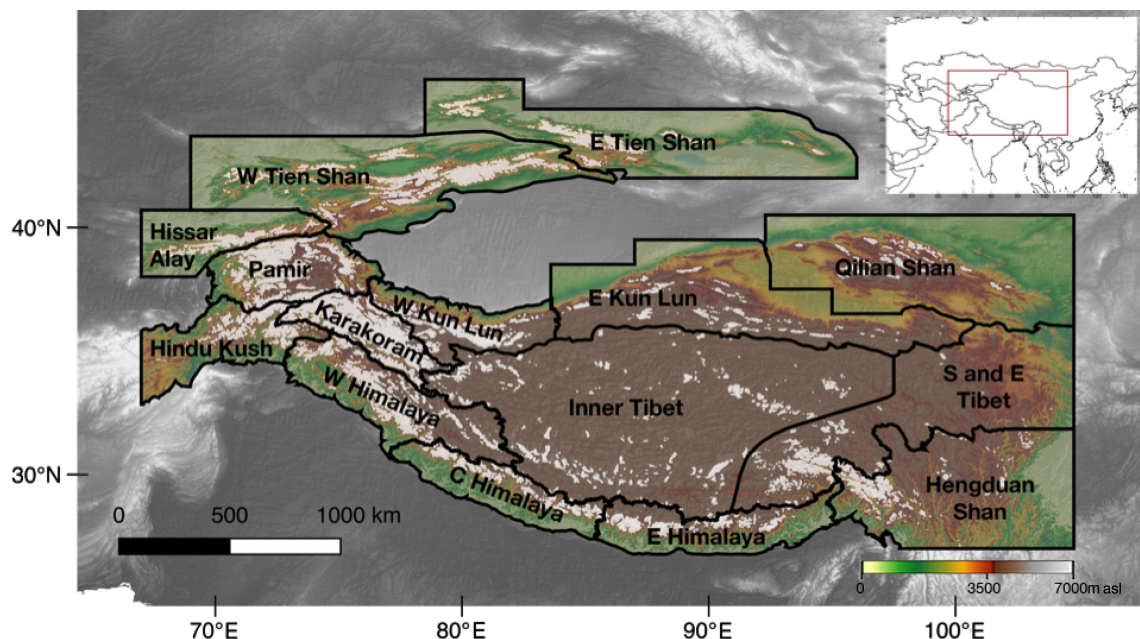


FIGURE 1 Regions for analysis with its topography and glaciers (white, RGI) with S, south; E, east; W, west

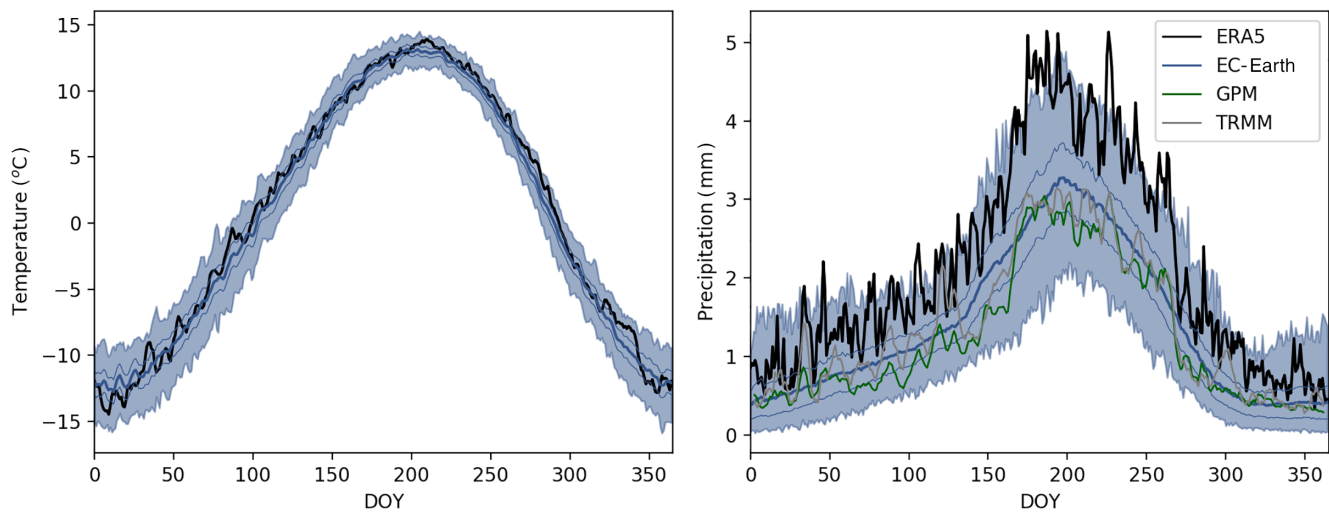


FIGURE 2 Average simulated daily temperature (left) and precipitation (right) for 2011–2015 for biascorrected EC-Earth (blue; 5-year average of 1,000 times random selection of 5 years in the large ensemble) and ERA5 (black). The 5-year average ensemble represents the spread in outcomes of present day large ensemble. Blue shading indicates minimum and maximum values; the thin line is the standard deviation

generally underestimate precipitation due to their spatial resolution and quality (Immerzeel *et al.*, 2015). Since the bias-corrected EC-Earth falls well within range of other gridded climate products and correctly captures the seasonality of precipitation we conclude that this product is suitable to use for climate impact studies in HMA.

3.2 | Changes in mean monthly temperature and precipitation

Temperature rise is not uniform over the year and regional differences are present (Figure 3). The global mean surface temperature in a 2C warmer world is 2°C warmer compared with pre-industrial levels; hence the changes with regard to PD are logically less than 2°C.

Compared to the global average (1.5 K, 3% increase P), HMA (1.5 K, 5.2% increase P) is projected to warm at a similar rate and is projected to become wetter in a 2C warmer world compared to PD climate. In a 3C warmer world regional differences become slightly more pronounced, with an average temperature rise of 2.9 K in HMA, while 2.7 K globally. Precipitation increases in HMA are substantially larger (13%) compared to the global average (5.9%). Regions with strongest precipitation increases are the Himalayas (23%), and Hengduan Shan (21%) regions.

The 2C warmer world shows a rather uniform warming in all regions (1.3 K in Hengduan Shan to 1.7 K in Hindu Kush), while the 3C warmer world shows distinct differences (1.4 K in West Kun Lun and 5 K in East Himalaya). However, regional averages are shown and the temperature signal in West Kun Lun region for

example is both negative and positive, resulting in a low regionally averaged temperature increase. A different sensitivity to processes causing elevation dependent warming can cause the differences per region (Pepin *et al.*, 2015). The strongest warming rates can be found in the south-eastern regions (Himalayas, Hindu Kush and Hengduan Shan).

Elevation dependent warming is the phenomenon that the rate of warming generally increases with elevation and is caused by local mechanisms that amplify global warming. Important mechanisms are for example the snow albedo feedbacks and water vapour changes. The differences in the local importance of each of these individual mechanisms result in contrasting regional patterns to global warming. In our simulations we can study the differences in temperature for the different climates and therefore identify the regions with largest changes in climate.

Elevation dependent warming is not observed in all regions of HMA in a 2C or 3C warmer world, however in specific regions and seasons it is (Figure 3). This could be an indication that the mechanisms behind elevation dependent warming are indeed region and time specific. Coarse resolution would not explain this, since previous studies showed that elevation dependent warming is also resolved at coarse resolution; however, the relative contribution of the driving mechanisms may differ in simulations with different spatial resolution (Rangwala *et al.*, 2016; Palazzi *et al.*, 2019). Physical processes contributing to elevation dependent warming include snow-albedo feedback, changes in clouds, sensitivity of downward longwave radiation to specific humidity and sensitivity of outgoing longwave

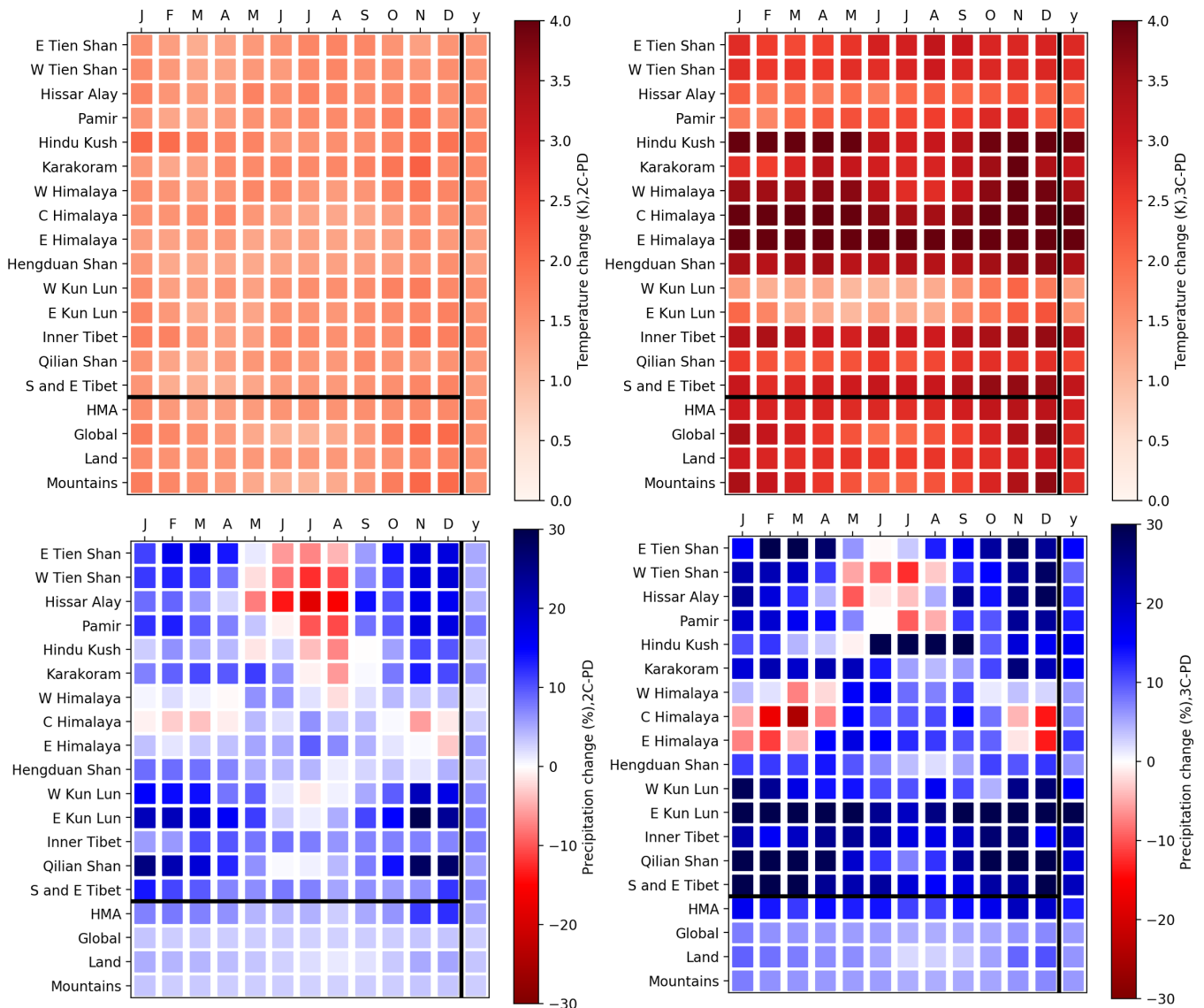


FIGURE 3 Temperature (upper panels) and precipitation (lower panels) anomalies for the 2C (left panels) and 3C (right panels) warmer world compared to present day climate. Columns indicate the individual months, and y = year average, rows indicate the region. Mountains are defined as all grid cells above 1,500 m (global)

radiation to surface temperature, aerosols and black carbon (Pepin *et al.*, 2015). Those processes also interact and can compensate each other (Pepin *et al.*, 2015; Gao *et al.*, 2018). In a 3C warmer world elevation dependent warming is observed in the Hindu Kush, West Himalaya, Central Himalaya, East Himalaya, Hengduan Shan and Inner, South and East Tibet. In West and East Kun Lun some sub-regions experience a temperature decrease, indicating elevation dependent warming is non-linear and complex. Additionally to the physical processes, also changes in circulation (e.g., monsoon strengthening in Himalayas) and snow cover changes (e.g., Tibet) play an important role in elevation dependent warming.

For precipitation we observe an overall wetting of HMA between PD and a 2C and 3C warmer world. We

also observe contrasting seasonal and regional signals. For example, the monsoon is strengthening in the Himalayas, while precipitation during the winter is decreasing. As a result differences between the wet and dry seasons are increasing (Lutz *et al.*, 2014; Biemans *et al.*, 2019). Overall, the differences in precipitation between PD and the 2C and 3C warmer worlds are spatially more heterogeneous and more profound than the temperature signals.

The Hindu Kush monsoon precipitation is projected to increase most in a 3C warmer world, which could be linked to strengthening and further protruding of the monsoon (Li *et al.*, 2010). In the north-western regions (Hissar Alay, Pamir, West Tien Shan and East Tien Shan) winter precipitation is projected to increase, while summer precipitation is projected to decrease. This is likely caused by an

intensification or increased occurrence of intense cyclones in winter (Lambert, 1995) and the orographic effect that results in more precipitation at the leeward side of the mountains (e.g., the Hindu Kush mountain range). The decrease in precipitation in a 2C warmer world is likely caused by the reduced moisture transport from the Mediterranean or projected reduced monsoon circulation, while in the 3C warmer world the intensification of the monsoon circulation dominates (Christensen *et al.*, 2013). This reversed signal is also found in model ensemble averages in the Upper Indus region, with a dominantly drying signal in 2071–2100 compared to 1971–2000 in RCP4.5, while a wettening signal in RCP8.5 (Lutz *et al.*, 2016). Precipitation changes are not linear with global temperature rise; for example a drying trend during the monsoon months is simulated in a 2C warmer world in Hindu Kush, Karakoram and West Himalaya, while the same regions are projected to become wetter in a 3C warmer world.

The Clausius-Claperyon relation predicts an increase in precipitation of $6.5\% \text{ K}^{-1}$ if precipitation is not constrained by the amount of moisture or energy (Allen and Ingram, 2002; Trenberth *et al.*, 2003; Held and Soden, 2006). Most climate models predict a global mean increase in precipitation of $1\text{--}3\% \cdot \text{K}^{-1}$ (Boer, 1993; Allen and Ingram, 2002; Stephens and Ellis, 2008; Trenberth, 2011). In this study we found a global mean precipitation increase of $2\% \cdot \text{K}^{-1}$, which is in line with the global CMIP projections. The precipitation increase in HMA is however between 3.5 and $4.6\% \cdot \text{K}^{-1}$, which is much closer to the theoretical Clausius-Clapeyron value. The high moisture availability and high temperatures during the monsoon season likely cause the strong precipitation increase with temperature in HMA.

3.3 | Return periods of temperature and precipitation

Mean temperature and precipitation are increasing due to global warming and likely return levels of extreme temperatures and precipitation too (Papalexiou and Montanari, 2019; Figure 4). Overall, the patterns in extremes are indeed in line with the annual trends in temperature and precipitation, where extreme temperatures and more intense precipitation events occur more frequently in a 2C and 3C warmer world compared to PD climate. The largest changes in return periods of daily averaged temperature extremes are observed in the southern regions and southern part of the Tien Shan region. Extreme precipitation is mostly changing in monsoon-dominated areas and higher elevated regions such as the Pamir and Karakoram. Interesting is that return periods of the most extreme events (1 in 100 years) change more

rapidly than less extreme return periods. Strengthening of the monsoon is causing the increase in precipitation extremes in the monsoon areas (see Section 3.4), while in higher elevated areas the increased moisture capacity effect in combination with the orography plays a role. Additionally a more erratic precipitation distribution can cause the increase in precipitation extremes (Krishna Kumar *et al.*, 2011; Sharmila *et al.*, 2015).

Return periods of daily averaged temperature show large spatial differences in south-eastern HMA, where PD 1:100 year events will change to multi-year events in a 3°C warmer world (Figure 4). This increase in daily averaged temperature events is severe. We would like to stress that the return periods are calculated with the averaged daily temperature and return periods of daily maximum temperature would not follow the same trend by definition. In the Hindu Kush PD 1:100 year temperature events (25°C) will occur in a 3C warmer world 1:2 years, whereas in the Karakoram (14°C) 1:1 years and in East Himalaya (15°C) 1:0.02 years.

Return periods of daily precipitation sums show a similar spatial pattern as daily averaged temperature events but its absolute change in return periods is significantly less. This difference in response is caused by the variability of daily averaged temperature and daily precipitation sums. The empirical distribution estimate (Figure S2) of daily averaged temperature is relatively flat between return periods of 1 and 100 years, resulting in large changes in return periods in a 2C and 3C warmer world. For example an event with a return period of 100 years in PD climate ($\pm 16^\circ\text{C}$) will occur yearly in a 3°C warmer world for that specific location. The extreme temperature events in a 3C warmer world are almost all higher than the most extreme values of PD temperatures, resulting in strong decreases in return periods with warmer climate. In the Hindu Kush PD 1:100 year precipitation events ($10 \text{ mm} \cdot \text{day}^{-1}$) will occur in a 3C warmer world 1:35 years, whereas in the Karakoram ($3 \text{ mm} \cdot \text{day}^{-1}$) 1:19 years and in East Himalaya ($0.11 \text{ mm} \cdot \text{day}^{-1}$) 1:8 years.

Overall, changes in return periods of precipitation extremes are largely homogeneous in a 2C warmer world, while regional differences are large in a 3C warmer world. This indicates that changes in return periods of temperature and precipitation are not linearly correlated with global temperature rise. For example, the change in return periods of temperature extremes in the south-western regions are only marginally affected in a 2C warmer world, while in a 3C warmer world those are heavily affected. As a consequence, this inhomogeneity will also lead to different regional changes in the number of natural hazards of for example landslides and flash floods. Detailed information of return periods is needed for an adequate prediction of extreme river discharge and

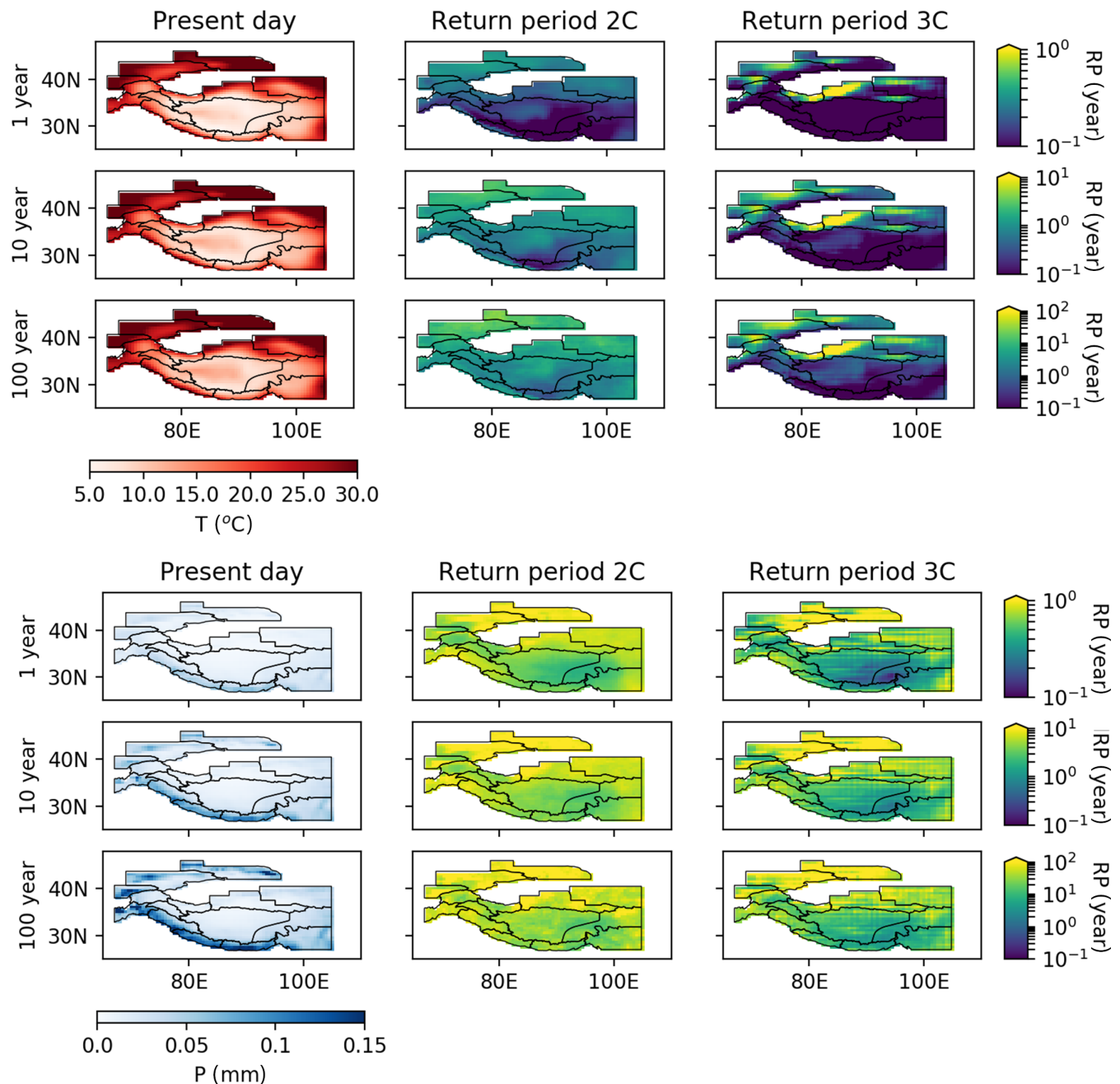


FIGURE 4 Daily averaged temperature and daily precipitation sums for different return periods (1, 10 and 100 years) for present day climate (left panels) and its new return periods (RP) in a 2C (middle panels) and 3C warmer world (right panels). Please note the different colorbars for the new return periods

likely has large consequences for the occurrence of floods and the production of hydropower.

3.4 | Mountain relevant climate indicators

Climate indicators reveal specific effects of global warming and can be used to study the regional sensitivity (of the cryosphere) to climate change. In Figure 5 changes in several

mountain climate indicators, which are proxies for natural hazards and cryospheric change are shown for HMA.

The PDD sum (Figure 5a) is a proxy for glacier melt and shows largest changes at the margins of HMA. It is interesting that relatively low-lying areas such as the southern part of HMA and Tien Shan show the strongest increasing trend. The snow-albedo effect can be of great importance in those areas, as strongest temperature changes are often found near the 0°C isotherm (Pepin and Lundquist, 2008).

Snowfall drives glacier accumulation (Figure 5b) and will decrease throughout HMA in a warmer world. Two effects are at play: a decrease in solid precipitation due to increasing temperatures and an increase in precipitation by the increased moisture holding capacity of the air at higher temperatures. The decrease in solid precipitation (Figure 5b) indicates that on a yearly basis the temperature effect is larger than the associated increase in total precipitation. The amount of solid precipitation (Figure 5b) is largest in the western regions, while largest changes can be found along the southern margin of the Himalayas. In the Karakoram, West Kunlun and Pamir regions minor changes are projected, which is in agreement with previous findings on the Karakoram anomaly (e.g., Farinotti *et al.*, 2020). We note that the spatial resolution of EC-Earth is insufficient to capture valley-scale processes, such as small-scale orographically forced precipitation, which is important for the distribution of temperature, precipitation and wind over short horizontal distances in mountainous terrain (Bonekamp *et al.*, 2018).

Pre-monsoon precipitation (Figure 5c) is expected to increase most in Central and East Himalaya, indicating an earlier onset of the monsoon. Changes are moderate in a 2C warmer world, while in a 3C warmer world a clear distinction is visible between the south-eastern regions (East Himalaya and Hengduan Shan and Southern Tibet) and the other regions. This is in correspondence with observed increases in pre-monsoon precipitation during last decades (Brunello *et al.*, 2019).

Monsoon precipitation (Figure 5d) is gradually intensifying in a 2C warmer world, while in a 3C warmer world a more heterogeneous pattern is visible, with distinct maxima in the Hindu Kush and East Tien Shan. The post-monsoon precipitation changes (Figure 5e) are largest in the north-western regions in a 2C warmer world, while in a 3C warmer world also in changes in East Himalaya, Hengduan Shan and South Tibet are substantial. Precipitation will increase in (pre- and post-) monsoon.

The change in the 95th percentile of temperature (Figure 5f) will be largely homogeneous in a 2C warmer world, but spatially variable in a 3C warmer world. The pattern of the PD temperature extremes is similar compared to the pattern of PDD, however the changes are not. Extreme temperatures change most in moderate temperature regimes (e.g., southern flanks of the Himalayas and Tien Shan) and change least in areas with high temperature extremes (e.g., Hissar Alay, Tien Shan). Interesting is the projected decline in temperature extremes in East and West Kunlun Shan, where also glaciers with stable or positive mass balance are found (Brun *et al.*, 2017).

Extreme precipitation (Figure 5g) increases absolutely the most in monsoon regions, and agrees with the

intensification of the monsoon circulation (Figure 5d). The monsoon intensification and monsoon region expansion also result in an increase in events where extreme temperature and extreme precipitation coincide (Figure 5h). Regions outside the monsoon-dominated areas generally receive their precipitation extremes in winter and their temperature extremes in summer. As a result, compound events are less common outside monsoon-dominated regions and therefore also less likely to change.

Our results are in accordance with Jury *et al.* (2019), who downscaled a climate model ensemble in order to assess the model uncertainty in 2-m temperature, PDD, accumulated precipitation and precipitation rate. They also found a decrease in solid precipitation, increase in monsoon precipitation and a PDD increase in lower elevated areas.

East Himalaya shows the strongest changes in all climate indicators, except the post-monsoon precipitation (Figure 6). Other regions with large changes are Tibet, Central Himalaya, East Himalaya, Hindu Kush and Hengduan Shan. The Karakoram, Qilian Shan and East and West Kun Lun are regions with the least change. We also observe that climate indicators changes are non-linear. For example in East Himalaya, the post-monsoon precipitation increases only marginally, while the extreme precipitation increase is large. Also the boreal summer precipitation in the Pamir did decrease in a 3C warmer world compared to a 2C warmer world. This non-linear effect can indicate tipping point behaviour in the climate system, located between 2C and 3C.

In Hengduan Shan and East Himalaya the pre-monsoon, monsoon and post-monsoon monsoon precipitation indicators change similarly, while in Central and West Himalaya the pre-monsoon precipitation changes more than the post-monsoon precipitation. In the 2C warmer world, changes in precipitation indicators are similar between the regions, while in a 3C warmer world changes become more distinct between the regions. Largest changes can be found in the monsoon-dominated areas and indicate that shifts in large-scale monsoon circulation are a key driver in this part of HMA.

3.5 | DT sensitivity per region for the relevant indicators

Not all regions show a similar sensitivity to the regional temperature increase. For all climate indicators the spatial heterogeneity in temperature change is lower in the 2C warmer world than in a 3C warmer world (Figure 7). In general, our results show that the

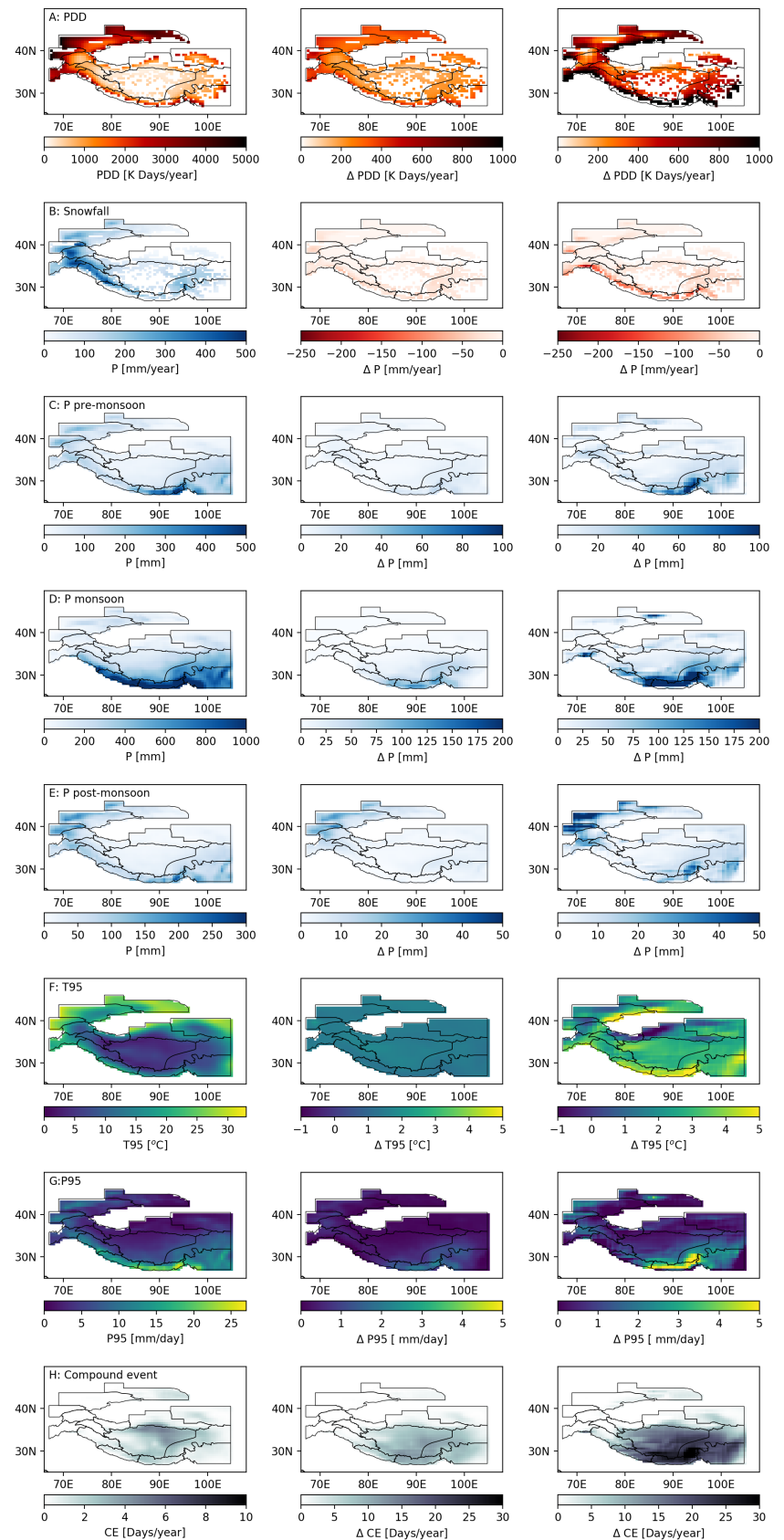


FIGURE 5 The different climate indicators for present day climate (left panels) and the anomaly of the 2C (middle panels) and 3C (right panels) warmer world compared to present day climate. Positive degree days and solid precipitation are only shown for glacier and/or snow covered areas for at least one month a year. Panel (a) positive degree days, (b) snowfall, (c–e) precipitation in pre-monsoon, monsoon and postmonsoon, (f, g) 95th percentile of temperature and precipitation, (h) compound events (95th percentile of temperature and precipitation)

climate indicators are positively correlated with the regional temperature increase. Only solid precipitation has a negative correlation with temperature. Lutz

et al. (2018) found a linear relationship for similar climate indicators for downstream areas (Indus, Ganges, Brahmaputra).

Monsoon precipitation changes the most of the precipitation indicators. Note that the monsoon precipitation is a precipitation sum over 4 months, while the pre-monsoon and post-monsoon precipitation is accumulated over 2 months. The monsoon precipitation ($+26 \text{ mm} \cdot \text{K}^{-1}$ or

$5.4\% \cdot \text{K}^{-1}$) and pre-monsoon ($+6 \text{ mm} \cdot \text{K}^{-1}$ or $2.0\% \cdot \text{K}^{-1}$) precipitation show a clear relation with different warming rates, while the post-monsoon precipitation shows a less clear and weaker signal ($1 \text{ mm} \cdot \text{K}^{-1}$ or $-0.5\% \cdot \text{K}^{-1}$). The significance of these relations is hard to quantify as

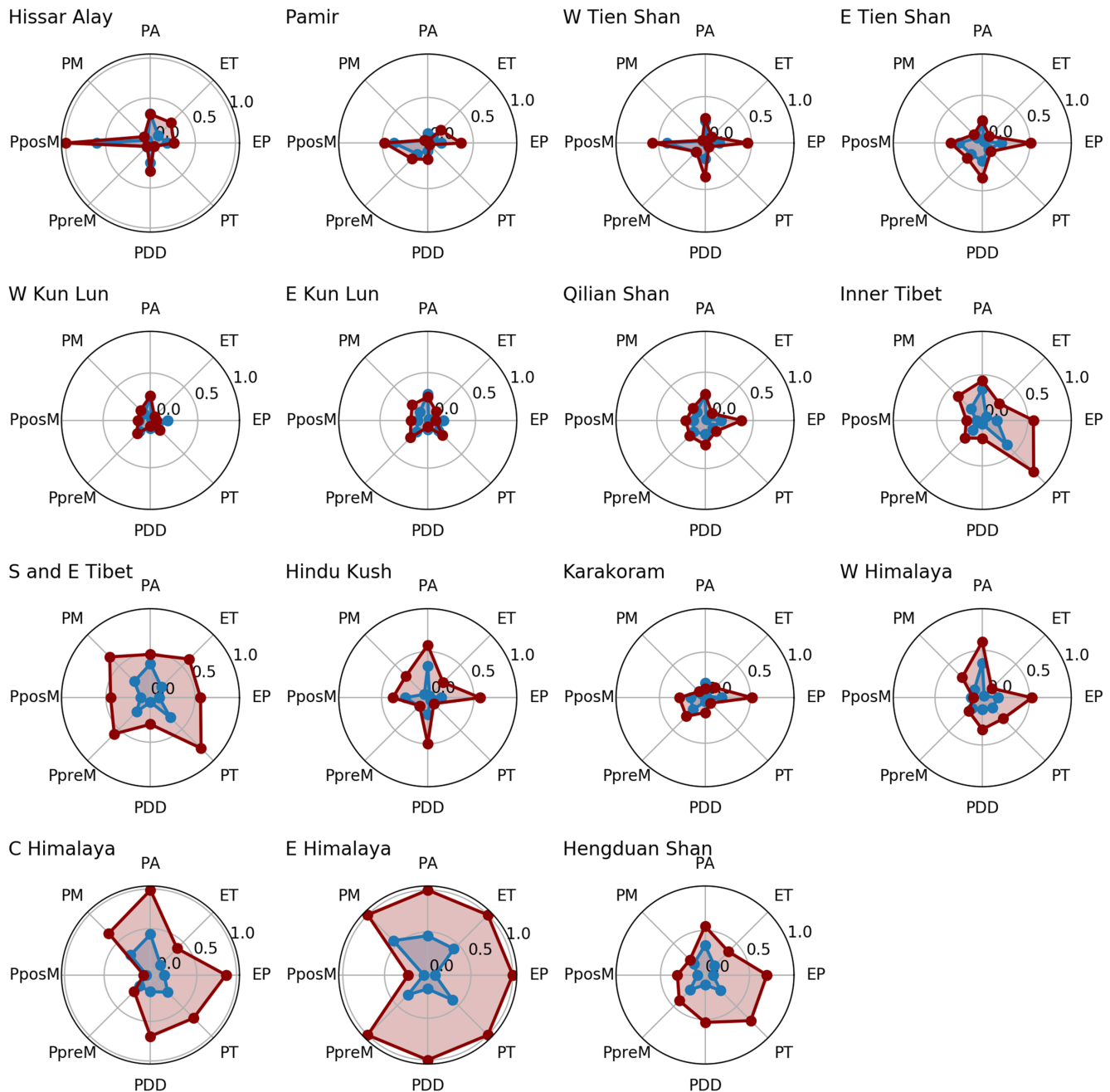


FIGURE 6 Regional summary of change in climate indicators compared to present day, normalized by the 3° warmer world. Each climate indicator is normalized by the maximum regional value: a value of 1 for a specific region and climate indicator means this climate indicator changed the most in that region compared to the other regions, EP, extreme precipitation (P95); ET, extreme temperature (T95); MD, melt days; PA, yearly solid precipitation sum; PpreM, precipitation during pre-monsoon; PM, monsoon precipitation; PposM, precipitation during post-monsoon; PDD, positive degree days; PT, compound event when both precipitation and temperature exceed the present day 95% percentile. The climate indicator change between 2°C and present day is indicated in blue, the change between 3°C and present day in red. Data are aggregated using all cells in a region, except for PDD and PA, where only glacier and/or snow-covered (at least 1 month a year) cells are considered

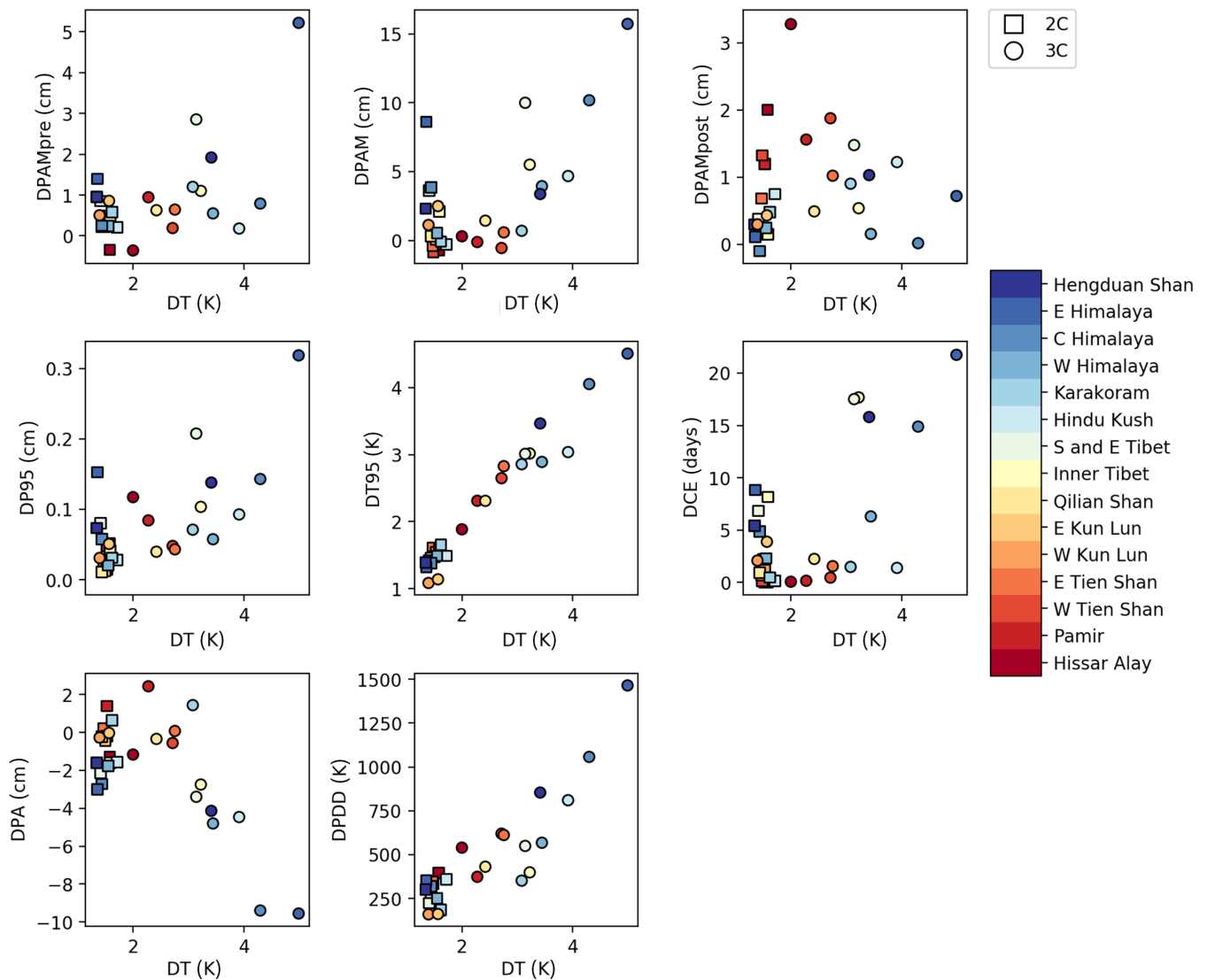


FIGURE 7 Regional climate indicators as a function of the change in average temperature for snow and glacier cells only. The squares denote the 2C warmer world and the dots a 3C warmer world. The difference in temperature between the 2C and 3C warmer world compared to present day is indicated on the x-axis (DT) and the difference in climate indicators on the y-axis: DPAMpre, precipitation during pre-monsoon; DPAM, monsoon precipitation; DPAMpost, post-monsoon precipitation; DP95, 95th percentile of precipitation; DT95, 95th percentile of temperature; DCE, compound events (when both precipitation and temperature exceed the present day 95% percentile); DPA, solid precipitation; DPDD, positive degree days

the temperature differences are small in a 2C world and the number of regions are low.

When we assume a linear relation between change in regional temperature and the climate indicators in Figure 7, precipitation extremes are projected to increase with $0.5 \text{ mm} \cdot \text{K}^{-1}$, temperature extremes with $0.87 \text{ K} \cdot \text{K}^{-1}$ and resulting compound events with $3.9 \text{ days} \cdot \text{K}^{-1}$, with strongest changes in the south-eastern part of HMA. Compound events are important for flooding, as those are indicative of periods where extreme rainfall coincides with periods of extreme melt. Accumulated solid precipitation is expected to decrease ($-1.9 \text{ cm} \cdot \text{K}^{-1}$), with strongest decreases in the Himalaya and Hindu Kush. The PDDs

are expected to increase with $256 \text{ days} \cdot \text{K}^{-1}$ per degree warming.

4 | CONCLUSION

In this study we have quantified projected changes in extreme weather events and climate indicators in HMA due to global climate changes. To this end, we used three large model ensembles of the EC-Earth model with 2000 simulation years in each ensemble (PD climate and in a 2C and 3C warmer world). The most important benefit of large ensemble modelling is that extreme events are

explicitly modelled, so no assumptions on tail behaviour of the distributions are required, and that results therefore have greater precision when analysing extreme events in HMA.

Using global climate model data to assess changes in mountainous climate is challenging, as the resolution is too coarse to resolve the complex topography and as a result resolving valley scale dynamics is generally not possible (Cannon *et al.*, 2017; Bonekamp *et al.*, 2018). However, GCMs allow us to generate large ensembles as used in this study due to their relatively low computational costs. Despite its coarse resolution, such an analysis provides key insights in how future extremes and mountain specific weather indicators may change at the large scale that would otherwise not be available.

Our results show that temperature and precipitation will not change uniformly. There are strong seasonal and regional differences between a 2C and 3C warmer world. Temperature will increase the most in Eastern HMA (Hindu Kush, Himalayas, Hengduan Shan, Tibet), while precipitation changes follow a more erratic trend. Winters in the Himalayas will be dryer, while wetter in other regions. Summers in the Tien Shan, Hissar Allay and Pamir regions will be dryer, while wetter in the rest of HMA. Elevation dependent warming in EC-Earth is only observed in the southern regions of HMA, and not in other regions. This would indicate elevation dependent warming is region specific and not solely an elevation-dependent effect.

The return periods of extreme temperature and precipitation events decrease in a warmer climate, and low-frequent events change more than less frequent events. The 1:100 years temperature events in PD climate will occur approximately yearly in a 2C warmer world (with a hot spot in Eastern Himalaya), and multi-yearly in a 3C warmer world in southern and central regions. Return periods of precipitation events show a similar spatial pattern as for temperature events but its absolute return period is considerably less. Precipitation changes are also notable in higher elevated regions such as the Pamir and Karakoram likely due to the increased moisture holding capacity of the atmosphere in combination with the high altitude climate.

We show that the global temperature rise has a large influence on the mountain-specific climate indicators in HMA. The increase in PDDs and decrease in solid precipitation will lead to more negative glacier mass balances, with largest effects in the Himalaya and Hengduan Shan regions. A 2C warmer world shows a rather homogeneous response, while distinct differences between regions are present in a 3C warmer world. This observation can indicate a non-linear acceleration in the regional climate system.

Differences between wet and dry seasons are amplified in monsoon-dominated regions by a dryer winter and wetter monsoon period in the future compared to present-day climate. Precipitation amounts will decrease in pre-monsoon in Hissay Alley, West Tien Shan, Hindu Kush and West and Central Himalaya, which will have large impact on the water availability during the growing season in downstream regions. Extreme temperature and precipitation are projected to increase the most in the Himalayas, southern part of Tien Shan and western regions. Compound events however are projected to increase most in monsoon-dominated areas, since temperature and precipitation extremes coincide. Overall, largest changes in climate indicators can be found in regions that are densely populated such as the Hindu Kush and Himalaya. East Himalaya is out far the most affected region, where seven out of eight climate indicators change the most, indicating climate change impacts this region the most.

The increase in weather extremes will affect the number and intensity of natural hazards and will increase the exposure to these hazards for all mountain communities' inhabitants directly. Our results are of great importance for climate change adaptation strategies in HMA and future research into the changes in meteorological and hydrological extremes in HMA is of key importance. Future research should focus on making the explicit link between climate model derived changes in extremes and impact models of natural hazards. This approach has been initiated for landslides in HMA (Kirschbaum *et al.*, 2020), but a full probabilistic approach using large ensemble modelling would be a logical and much needed next step.

ACKNOWLEDGEMENTS

This project has received funding from the European Research Council (ERC) under the European Union Horizon 2020 Research and Innovation Program (Grant Agreement No. 676819) and Netherlands Organization for Scientific Research under the Innovational Research Incentives Scheme VIDI (Grant Agreement No. 016.181.308). N. W. acknowledges funding by NWO 016.Veni.181.049. K. W. acknowledges the HiWAVES3 project for which funding was supplied by the Netherlands Organisation of Scientific Research (NWO) under Grant Number ALWCL.2016.2. Supercomputing resources were financially supported by NWO and provided by SURFsara (www.surfsara.nl) on the Cartesius cluster.

ORCID

P. N. J. Bonekamp  <https://orcid.org/0000-0002-7954-6510>

REFERENCES

- Allen, M.R. and Ingram, W.J. (2002) Constraints on future changes in climate and the hydrologic cycle. *Nature*, 419, 228–232. <https://doi.org/10.1038/nature01092>.
- Aznar-Siguan, G. and Bresch, D.N. (2019) CLIMADA v1: a global weather and climate risk assessment platform. *Geoscientific Model Development*, 12, 3085–3097. <https://doi.org/10.5194/gmd-12-3085-2019>.
- Biemans, H., Siderius, C., Lutz, A.F., Nepal, S., Ahmad, B., Hassan, T., von Bloh, W., Wijngaard, R.R., Wester, P., Shrestha, A.B. and Immerzeel, W.W. (2019) Importance of snow and glacier meltwater for agriculture on the Indo-Gangetic Plain. *Nature Sustainability*, 2, 594–601. <https://doi.org/10.1038/s41893-019-0305-3>.
- Boer, G.J. (1993) Climate change and the regulation of the surface moisture and energy budgets. *Climate Dynamics*, 8, 225–239. <https://doi.org/10.1007/BF00198617>.
- Bonekamp, P.N.J., Collier, E. and Immerzeel, W.W. (2018) The impact of spatial resolution, landuse and spin-up time on resolving spatial precipitation patterns in the Himalayas. *Journal of Hydrometeorology*, 19(10), 1565–1591. <https://doi.org/10.1175/JHM-D-17-0212.1>.
- Brun, F., Berthier, E., Wagnon, P., Kääb, A. and Treichler, D. (2017) A spatially resolved estimate of High Mountain Asia glacier mass balances from 2000 to 2016. *Nature Geoscience*, 10(9), 668–673. <https://doi.org/10.1038/ngeo2999>.
- Brunello, C.F., Andermann, C., Helle, G., Comiti, F., Tonon, G., Tiwari, A. and Hovius, N. (2019) Hydroclimatic seasonality recorded by tree ring $\delta^{18}\text{O}$ signature across a Himalayan altitudinal transect. *Earth and Planetary Science Letters*, 518, 148–159. <https://doi.org/10.1016/j.epsl.2019.04.030>.
- Buizza, R., Miller, M. and Palmer, T.N. (1999) Stochastic representation of model uncertainties in the ECMWF ensemble prediction system. *Quarterly Journal of the Royal Meteorological Society*, 125, 2887–2908. <https://doi.org/10.1025/smsqj.56005>.
- Cannon, F., Carvalho, L.M.V., Jones, C., Norris, J., Bookhagen, B. and Kiladis, G.N. (2017) Effects of topographic smoothing on the simulation of winter precipitation in High Mountain Asia. *Journal of Geophysical Research*, 122(3), 1456–1474. <https://doi.org/10.1002/2016JD026038>.
- Christensen, J.H., Kumar, K.K., Aldrian, E., An, S.-I., Cavalcanti, I. F.A., de Castro, M., Dong, W., Goswami, P., Hall, A., Kanyanga, J.K., Kitoh, A., Kossin, J., Lau, N.-C., Renwick, J., Stephenson, D.B., Xie, S.-P. and Zhou, T. (2013) In: Stocker, T. F., Qin, D., Plattner, G.-K., Tignor, M., Allen, S.K., Boschung, J., Nauels, A. and Xia, Y. (Eds.) *Climate Change 2013: The Physical Science Basis: Working Group I Contribution to the Fifth Assessment Report of the Intergovernmental Panel on Climate Change*. Cambridge, United Kingdom/New York, NY: Cambridge University Press.
- Copernicus Climate Change Service (C3S) (2017) ERA5: fifth generation of ECMWF atmospheric reanalyses of the global climate. Copernicus Climate Change Service Climate Data Store (CDS). Available at: <https://cds.climate.copernicus.eu/cdsapp#!/home>.
- Dai, A. (2006) Precipitation characteristics in eighteen coupled climate models. *Journal of Climate*, 19, 4605–4630. <https://doi.org/10.1175/JCLI3884.1>.
- Farinotti, D., Immerzeel, W.W., de Kok, R.J., Quincey, D.J. and Dehecq, A. (2020) Manifestations and mechanisms of the Karakoram glacier anomaly. *Nature Geoscience*, 13(January), 8–16. <https://doi.org/10.1038/s41561-019-0513-5>.
- Gao, Y., Chen, F., Lettenmaier, D.P., Xu, J., Xiao, L. and Li, X. (2018) Does elevation-dependent warming hold true above 5000m elevation? Lessons from the Tibetan Plateau. *NPJ Climate and Atmospheric Sciences*, 9, 1–19. <https://doi.org/10.1038/s41612-018-0030-z>.
- Hall, D. K. and Riggs, G. A (2015) *MODIS/Terra snow cover monthly L3 global 0.05Deg CMG, version 6*. Boulder, CO.
- Hauser, M., Gudmundsson, L., Orth, R., Jézéquel, A., Haustein, K., Vautard, R., van Oldenborgh, G.J., Wilcox, L. and Seneviratne, S.I. (2017) Methods and model dependency of extreme event attribution: the 2015 European drought. *Earth's Future*, 5, 1034–1043. <https://doi.org/10.1002/2017EF000612>.
- Hazeleger, W., Van Den Hurk, B.J.J.M., Min, E., Van Oldenborgh, G.J., Petersen, A.C., Stainforth, D.A., Vasileiadou, E. and Smith, L.A. (2015) Tales of future weather. *Nature Climate Change*, 5, 107–113. <https://doi.org/10.1038/nclimate2450>.
- Hazeleger, W., Wang, X., Severijns, C., Steffenescu, S., Bintanja, R., Sterl, A., Wyser, K., Semmler, T., Yang, S., van den Hurk, B., van Noije, T., van der Linden, E. and van der Wiel, K. (2012) EC-Earth V2.2: description and validation of a new seamless earth system prediction model. *Climate Dynamics*, 39(11), 2611–2629. <https://doi.org/10.1007/s00382-011-1228-5>.
- Held, I.M. and Soden, B.J. (2006) Robust responses of the hydrological cycle to global warming. *Journal of Climate*, 19, 5686–5699. <https://doi.org/10.1175/JCLI3990.1>.
- Huffman, G.J., Adler, R.F., Bolvin, D.T., Gu, G., Nelkin, E.J., Bowman, K.P., Hong, Y., Stocker, E.F. and Wolff, D.B. (2007) The TRMM multisatellite precipitation analysis (TMPA): quasi-global, multiyear, combined-sensor precipitation estimates at fine scales. *Journal of Hydrometeorology*, 8, 38–55. <https://doi.org/10.1175/JHM560.1>.
- Huffman, G., Bolvin, D. T., Braithwaite, D., Hsu, K., Joyce, R. and Xie, P. (2014) *NASA global precipitation measurement (GPM) integrated multi-satellite retrievals for GPM (IMERG), version 4.4*.
- Immerzeel, W.W., Lutz, A.F., Andrade, M., Bahl, A., Biemans, H., Bolch, T., Hyde, S., Brumby, S., Davies, B.J., Elmore, A.C., Emmer, A., Feng, M., Fernández, A., Haritashya, U., Kargel, J. S., Koppes, M., Kraaijenbrink, P.D.A., Kulkarni, A.V., Mayewski, P.A., Nepal, S., Pacheco, P., Painter, T.H., Pellicciotti, F., Rajaram, H., Rupper, S., Sinisalo, A., Shrestha, A.B., Viroli, D., Wada, Y., Xiao, C., Yao, T. and Baillie, J.E.M. (2020) Importance and vulnerability of the world's water towers. *Nature*, 577(7790), 364–369. <https://doi.org/10.1038/s41586-019-1822-y>.
- Immerzeel, W.W., Wanders, N., Lutz, A.F., Shea, J.M. and Bierkens, M.F.P. (2015) Reconciling high-altitude precipitation in the upper Indus basin with glacier mass balances and runoff. *Hydrology and Earth System Sciences*, 19(11), 4673–4687. <https://doi.org/10.5194/hess-19-4673-2015>.
- James, R., Washington, R., Schleussner, C.F., Rogelj, J. and Conway, D. (2017) Characterizing half-a-degree difference: a review of methods for identifying regional climate responses to global warming targets. *Wiley Interdisciplinary Reviews: Climate Change*, 8, 1–23. <https://doi.org/10.1002/wcc.457>.
- Jury, M.W., Mendlik, T., Tani, S., Truhetz, H., Maraun, D., Immerzeel, W.W. and Lutz, A.F. (2019) Climate projections for

- glacier change modelling over the Himalayas. *International Journal of Climatology*, 40, 1738–1754. <https://doi.org/10.1002/joc.6298>.
- Kirschbaum, D., Kapnick, S.B., Stanlet, T. and Pascale, S. (2020) Changes in extreme precipitation and landslides over High Mountain Asia. *Geophysical Research Letters*, 47(4), 1–9. <https://doi.org/10.1029/2019GL085347>.
- Kraaijenbrink, P.D.A., Bierkens, M.F.P., Lutz, A.F. and Immerzeel, W.W. (2017) Impact of a global temperature rise of 1.5 degrees Celsius on Asia's glaciers. *Nature*, 549, 257–260. <https://doi.org/10.1038/nature23878>.
- Krishna Kumar, K., Patwardhan, S.K., Kulkarni, A., Kamala, K., Koteswara Rao, K. and Jones, R. (2011) Simulated projections for summer monsoon climate over India by a high-resolution regional climate model (PRECIS). *Current Science*, 101(3), 312–326.
- Lambert, S.J. (1995) The effect of enhanced greenhouse warming on winter cyclone frequencies and strengths. *Journal of Climate*, 8, 1447–1452. [https://doi.org/10.1175/1520-0442\(1995\)008<1447:teoegw>2.0.co;2](https://doi.org/10.1175/1520-0442(1995)008<1447:teoegw>2.0.co;2).
- Li, J., Wu, Z., Jiang, Z. and He, J. (2010) Can global warming strengthen the East Asian summer monsoon? *Journal of Climate*, 23, 6696–6705. <https://doi.org/10.1175/2010JCLI3434.1>.
- Lutz, A.F., Immerzeel, W.W., Gobiet, A., Pellicciotti, F. and Bierkens, M.F.P. (2013) Comparison of climate change signals in CMIP3 and CMIP5 multi-model ensembles and implications for Central Asian glaciers. *Hydrology and Earth System Sciences*, 17(9), 3661–3677. <https://doi.org/10.5194/hess-17-3661-2013>.
- Lutz, A.F., Immerzeel, W.W., Kraaijenbrink, P.D.A., Shrestha, A.B. and Bierkens, M.F.P. (2016) Climate change impacts on the upper indus hydrology: sources, shifts and extremes. *PLoS One*, 11, e0165630. <https://doi.org/10.1371/journal.pone.0165630>.
- Lutz, A.F., Immerzeel, W.W., Shrestha, A.B. and Bierkens, M.F.P. (2014) Consistent increase in high Asia's runoff due to increasing glacier melt and precipitation. *Nature Climate Change*, 4(7), 587–592. <https://doi.org/10.1038/nclimate2237>.
- Lutz, A. F., Maat, H. W., Wijngaard, R. R., Biemans, H., Syed, A. and Shrestha, A. B.: South Asian river basins in a 1.5 °C warmer world, *Reg. Environ. Chang.*, (November), doi:<https://doi.org/10.1007/s10113-018-1433-4>, 2018.
- Nanditha, J., van der Wiel, K., Bhatia, U., Stone, D., Selton, F. and Mishra, V. (2020) A seven-fold rise in the probability of exceeding the observed hottest summer in India in a 2°C warmer world. *Environmental Research Letters*, 15(4), 1–12. <https://doi.org/10.1088/1748-9326/ab7555>.
- Palazzi, E., Mortarini, L., Terzaghi, S. and von Hardenberg, J. (2019) Elevation-dependent warming in global climate model simulations at high spatial resolution. *Climate Dynamics*, 52(5–6), 2685–2702. <https://doi.org/10.1007/s00382-018-4287-z>.
- Palazzi, E., Von Hardenberg, J. and Provenzale, A. (2013) Precipitation in the hindu-kush karakoram himalaya: observations and future scenarios. *Journal of Geophysical Research – Atmospheres*, 118(1), 85–100. <https://doi.org/10.1029/2012JD018697>.
- Papalexiou, S.M. and Montanari, A. (2019) Global and regional increase of precipitation extremes under global warming. *Water Resources Research*, 55(6), 4901–4914. <https://doi.org/10.1029/2018WR024067>.
- Pepin, N., Bradley, R.S., Diaz, H.F., Baraer, M., Caceres, E.B., Forsythe, N., Fowler, H., Greenwood, G., Hashmi, M.Z., Liu, X. D., Miller, J.R., Ning, L., Ohmura, A., Palazzi, E., Rangwala, I., Schöner, W., Severskiy, I., Shahgedanova, M., Wang, M.B., Williamson, S.N. and Yang, D.Q. (2015) Elevation-dependent warming in mountain regions of the world. *Nature Climate Change*, 5, 424–430. <https://doi.org/10.1038/nclimate2563>.
- Pepin, N.C. and Lundquist, J.D. (2008) Temperature trends at high elevations: patterns across the globe. *Geophysical Research Letters*, 35(14), 1–6. <https://doi.org/10.1029/2008GL034026>.
- Rangwala, I., Sinsky, E. and Miller, J.R. (2016) Variability in projected elevation dependent warming in boreal midlatitude winter in CMIP5 climate models and its potential drivers. *Climate Dynamics*, 46(6–8), 2115–2122. <https://doi.org/10.1007/s00382-015-2692-0>.
- RGI Consortium (2017) *Randolph Glacier Inventory – a dataset of global glacier outlines: version 6.0: technical report*. Global Land Ice Measurements from Space, Colorado, USA.
- Sharmila, S., Joseph, S., Sahai, A.K., Abhilash, S. and Chattopadhyay, R. (2015) Future projection of Indian summer monsoon variability under climate change scenario: an assessment from CMIP5 climate models. *Global and Planetary Change*, 124, 62–78. <https://doi.org/10.1016/j.gloplacha.2014.11.004>.
- Stephens, G.L. and Ellis, T.D. (2008) Controls of global-mean precipitation increases in global warming GCM experiments. *Journal of Climate*, 21, 6141–6154. <https://doi.org/10.1175/2008JCLI2144.1>.
- Tariq, S., Mahmood, A. and Rasul, G. (2014) Temperature and precipitation: GLOF triggering indicators in Gilgit-Baltistan, Pakistan. *Pakistan Journal of Meteorology*, 10(20), 39–56.
- Taylor, K.E., Stouffer, R.J. and Meehl, G.A. (2012) An overview of CMIP5 and the experiment design. *Bulletin of the American Meteorological Society*, 93(4), 485–498. <https://doi.org/10.1175/BAMS-D-11-00094.1>.
- Trenberth, K.E. (2011) Changes in precipitation with climate change. *Climate Research*, 47, 123–138. <https://doi.org/10.3354/cr00953>.
- Trenberth, K.E., Dai, A., Rasmussen, R.M. and Parsons, D.B. (2003) The changing character of precipitation. *Bulletin of the American Meteorological Society*, 84, 1205–1218. <https://doi.org/10.1175/BAMS-84-9-1205>.
- Trenberth, K.E., Fasullo, J.T. and Shepherd, T.G. (2015) Attribution of climate extreme events. *Nature Climate Change*, 5(8), 725–730. <https://doi.org/10.1038/nclimate2657>.
- Vos, F., Rodriguez, J., Below, R. and Guha-Sapir, D. (2010) *Annual Disaster Statistical Review 2009: the numbers and trends*, Brussels.
- Wester, P., Mishra, A., Mukherji, A. and Bhakta Shrestha, A. (2019) *The Hindu Kush Himalaya Assessment – Mountains, Climate Change, Sustainability and People*. Cham: Springer Nature Switzerland AG.
- van der Wiel, K., Wanders, N., Selten, F.M. and Bierkens, M.F.P. (2019) Added value of large ensemble simulations for assessing extreme river discharge in a 2°C warmer world. *Geophysical Research Letters*, 46(46), 2093–2102. <https://doi.org/10.1029/2019GL081967>.
- Wijngaard, R.R., Biemans, H., Friedrich Lutz, A., Bhakta Shrestha, A., Wester, P. and Willem Immerzeel, W. (2018)

Climate change vs. socio-economic development: understanding the future South Asian water gap. *Hydrology and Earth System Sciences*, 22, 6297–6321. <https://doi.org/10.5194/hess-22-6297-2018>.

SUPPORTING INFORMATION

Additional supporting information may be found online in the Supporting Information section at the end of this article.

How to cite this article: Bonekamp PNJ, Wanders N, van der Wiel K, Lutz AF, Immerzeel WW. Using large ensemble modelling to derive future changes in mountain specific climate indicators in a 2 and 3°C warmer world in High Mountain Asia. *Int J Climatol*. 2021;41 (Suppl. 1):E964–E979. <https://doi.org/10.1002/joc.6742>